Neutron Capture on the s-Process Branching Point ^{171}Tm via Time-of-Flight and Activation

C. Guerrero,[1,2,*] J. Lerendegui-Marco,[1] M. Paul,[3] M. Tessler,[4] S. Heinitz,[5] C. Domingo-Pardo,[6] S. Cristallo,[7,8] R. Dressler,[5] S. Halfon,[4] N. Kivel,[5] U. Köster,[9] E. A. Maugeri,[5] T. Palchan-Hazan,[3] J. M. Quesada,[1] D. Rochman,[5] D. Schumann,[5] L. Weissman,[4] O. Aberle,[10] S. Amaducci,[26] J. Andrzejewski,[11] L. Audouin,[12] V. Bécares,[13] M. Bacak,[14] J. Balibrea,[13] A. Barak,[4] M. Barbagallo,[15] S. Barros,[16] F. Bečvář,[17] C. Beinrucker,[18] D. Berkovits,[4] E. Berthoumieux,[19] J. Billowes,[20] D. Bosnar,[21] M. Brugger,[10] Y. Buzaglo,[4] M. Caamaño,[22] F. Calviño,[23] M. Calviani,[10] D. Cano-Ott,[13] R. Cardella,[10] A. Casanovas,[23] D. M. Castelluccio,[24,25] F. Cerutti,[10] Y. H. Chen,[12] E. Chiaveri,[10] N. Colonna,[15] G. Cortés,[23] M. A. Cortés-Giraldo,[1] L. Cosentino,[26] H. Dafna,[4] A. Damone,[15,27] M. Diakaki,[19] M. Dietz,[28] E. Dupont,[19] I. Durán,[22] Y. Eisen,[4] B. Fernández-Domínguez,[22] A. Ferrari,[10] P. Ferreira,[16] P. Finocchiaro,[26] V. Furman,[29] K. Göbel,[18] A. R. García,[13] A. Gawlik,[4] T. Glodariu,[30] I. F. Gonçalves,[16] E. González-Romero,[13] A. Goverdovski,[31] E. Griesmayer,[14] F. Gunsing,[19,9] H. Harada,[32] T. Heftrich,[18] J. Heyse,[23,43] T. Hirsh,[4] D. G. Jenkins,[34] E. Jericha,[14] F. Käppeler,[35] Y. Kadi,[10] B. Kaizer,[4] T. Katabuchi,[36] P. Kavrigin,[14] V. Ketlerov,[31] V. Khryachkov,[31] D. Kijel,[4] A. Kimura,[32] M. Kokkoris,[37] A. Kriesel,[4] M. Krtička,[17] E. Leal-Cidoncha,[22] C. Lederer-Woods,[28] H. Leeb,[14] S. Lo Meo,[24,25] S. J. Lonsdale,[28] R. Losito,[10] D. Macina,[10] A. Manna,[25,38] J. Marganiec,[11] T. Martínez,[13] C. Massimi,[25,38] P. Mastinu,[39] M. Mastromarco,[15] F. Matteucci,[40,41] E. Mendoza,[13] A. Mengoni,[24] P. M. Milazzo,[40] M. A. Millán-Callado,[1,2] F. Mingrone,[25] M. Mirea,[30] S. Montesano,[10] A. Musumarra,[26,42] R. Nolte,[43] A. Oprea,[30] N. Patronis,[44] A. Pavlik,[45] J. Perkowski,[11] L. Piersanti,[7] I. Porras,[46] J. Praena,[1,46] K. Rajeev,[47] T. Rauscher,[48,49] R. Reifarth,[18] T. Rodríguez-González,[1,2] P. C. Rout,[47] C. Rubbia,[10] J. A. Ryan,[20] M. Sabaté-Gilarte,[1,10] A. Saxena,[47] P. Schillebeeckx,[33] S. Schmidt,[18] A. Shor,[4] P. Sedyshev,[29] A. G. Smith,[20] A. Stamatopoulos,[37] G. Tagliente,[15] J. L. Tain,[6] A. Tarifeño-Saldivia,[23] L. Tassan-Got,[12] A. Tsinganis,[37] S. Valenta,[17] G. Vannini,[25,38] V. Variale,[15] P. Vaz,[16] A. Ventura,[25] V. Vlachoudis,[10] R. Vlastou,[37] A. Wallner,[50] S. Warren,[20] M. Weigand,[18] C. Weiss,[10,14] C. Wolf,[18] P. J. Woods,[28] T. Wright,[20] and P. Žugec[21,10]

(n_TOF Collaboration)

[1]Universidad de Sevilla, Seville, Spain
[2]Centro Nacional de Aceleradores (CNA) (Universidad de Sevilla-Junta de Andalucía-CSIC), Seville, Spain
[3]Hebrew University, Jerusalem, Israel
[4]Soreq Nuclear Research Center (SNRC), Yavne, Israel
[5]Paul Scherrer Institut (PSI), Villigen, Switzerland
[6]Instituto de Física Corpuscular (CSIC-University of Valencia), Valencia, Spain
[7]INAF-Osservatorio Astronomico d'Abruzzo, Teramo, Italy
[8]INFN Sezione Perugia, Perugia, Italy
[9]Institut Laue-Langevin ILL, Grenoble, France
[10]European Organization for Nuclear Research (CERN), Geneva, Switzerland
[11]University of Lodz, Lodz, Poland
[12]Institut de Physique Nucléaire, CNRS-IN2P3, Univ. Paris-Sud, Université Paris-Saclay, Orsay Cedex, France
[13]Centro de Investigaciones Energéticas Medioambientales y Tecnológicas (CIEMAT), Madrid, Spain
[14]Technische Universität Wien, Vienna, Austria
[15]Istituto Nazionale di Fisica Nucleare, Sezione di Bari, Italy
[16]Instituto Superior Técnico, Lisbon, Portugal
[17]Charles University, Prague, Czech Republic
[18]Goethe University Frankfurt, Seville, Germany
[19]CEA Irfu, Université Paris-Saclay, Gif-sur-Yvette, France
[20]University of Manchester, Manchester, United Kingdom
[21]Department of Physics, Faculty of Science, University of Zagreb, Zagreb, Croatia
[22]University of Santiago de Compostela, Santiago de Conpostela, Spain
[23]Universitat Politècnica de Catalunya, Barcelona, Spain
[24]Agenzia nazionale per le nuove tecnologie (ENEA), Bologna, Italy
[25]Istituto Nazionale di Fisica Nucleare, Sezione di Bologna, Italy
[26]INFN Laboratori Nazionali del Sud, Catania, Italy
[27]Dipartimento di Fisica, Università degli Studi di Bari, Bari, Italy
[28]School of Physics and Astronomy, University of Edinburgh, Edinburgh, United Kingdom

^{29}Joint Institute for Nuclear Research (JINR), Dubna, Russia
^{30}Horia Hulubei National Institute of Physics and Nuclear Engineering, Jerusalem, Romania
^{31}Institute of Physics and Power Engineering (IPPE), Obninsk, Russia
^{32}Japan Atomic Energy Agency (JAEA), Tokai-mura, Japan
^{33}European Commission, Joint Research Centre, Geel, Belgium
^{34}University of York, York, United Kingdom
^{35}Karlsruhe Institute of Technology (KIT), Karlsruhe, Germany
^{36}Tokyo Institute of Technology, Tokyo, Japan
^{37}National Technical University of Athens, Athens, Greece
^{38}Dipartimento di Fisica e Astronomia, Università di Bologna, Bologna, Italy
^{39}Istituto Nazionale di Fisica Nucleare, Sezione di Legnaro, Italy
^{40}Istituto Nazionale di Fisica Nucleare, Sezione di Trieste, Italy
^{41}Dipartimento di Astronomia, Università di Trieste, Trieste, Italy
^{42}Dipartimento di Fisica e Astronomia, Università di Catania, Catania, Italy
^{43}Physikalisch-Technische Bundesanstalt (PTB), Braunschweig, Germany
^{44}University of Ioannina, Ioannina, Greece
^{45}University of Vienna, Faculty of Physics, Vienna, Austria
^{46}University of Granada, Granada, Spain
^{47}Bhabha Atomic Research Centre (BARC), Mumbai, India
^{48}Centre for Astrophysics Research, University of Hertfordshire, Hatfield, United Kingdom
^{49}Department of Physics, University of Basel, Basel, Switzerland
^{50}Australian National University, Canberra, Australia

The neutron capture cross sections of several unstable nuclides acting as branching points in the s process are crucial for stellar nucleosynthesis studies. The unstable ^{171}Tm ($t_{1/2} = 1.92$ yr) is part of the branching around mass $A \sim 170$ but its neutron capture cross section as a function of the neutron energy is not known to date. In this work, following the production for the first time of more than 5 mg of ^{171}Tm at the high-flux reactor Institut Laue-Langevin in France, a sample was produced at the Paul Scherrer Institute in Switzerland. Two complementary experiments were carried out at the neutron time-of-flight facility (n_TOF) at CERN in Switzerland and at the SARAF liquid lithium target facility at Soreq Nuclear Research Center in Israel by time of flight and activation, respectively. The result of the time-of-flight experiment consists of the first ever set of resonance parameters and the corresponding average resonance parameters, allowing us to make an estimation of the Maxwellian-averaged cross sections (MACS) by extrapolation. The activation measurement provides a direct and more precise measurement of the MACS at 30 keV: 384 (40) mb, with which the estimation from the n_TOF data agree at the limit of 1 standard deviation. This value is 2.6 times lower than the JEFF-3.3 and ENDF/B-VIII evaluations, 25% lower than that of the Bao et al. compilation, and 1.6 times larger than the value recommended in the KADoNiS (v1) database, based on the only previous experiment. Our result affects the nucleosynthesis at the $A \sim 170$ branching, namely, the ^{171}Yb abundance increases in the material lost by asymptotic giant branch stars, providing a better match to the available pre-solar SiC grain measurements compared to the calculations based on the current JEFF-3.3 model-based evaluation.

The slow-neutron-capture (s) process is responsible for the synthesis of more than half of the elements heavier than iron in the Universe. The phenomenological picture of the classical s process was formulated 60 years ago in the seminal paper of Burbidge et al. [1], where the entire s-process panorama was already sketched in its essential parts. The study of this process involves detailed stellar modeling, constrained by spectroscopic observations and laboratory measurements, in which reliable information on the nuclear physics side, in particular on the half-lives and cross sections [2], constitutes essential ingredients. In this context, cross sections of unstable nuclides close to the valley of stability are of particular interest, as they may act as branching points along the s-process path where neutron capture and β decay become competing processes. As an illustrative example, Neyskens et al. [3] have recently been

able to determine an upper limit of 2.5×10^8 K for the s-process temperature in low-mass asymptotic giant branch (AGB) stars (see also Ref. [4]). This result has been possible thanks to a combination of the HERMES spectrograph observations [5] of the Zr/Nb abundance ratio in red giants and the availability of the new experimental Maxwellian-averaged cross sections (MACS) values of the long-lived ^{93}Zr neutron capture cross section measured at n_TOF [6].

Despite the importance of the neutron capture cross section of unstable isotopes in the s process [2], only a few have been measured by activation (^{135}Cs [7], ^{147}Pm [8,9], ^{155}Eu [10], ^{163}Ho [11], and ^{171}Tm [12]), and only two (^{63}Ni [13,14] and ^{151}Sm [15]), both with quite long half-lives of around 100 years, as functions of the neutron energy via the time-of-flight method.

Among the different branching points, the $A \sim 170$ region sketched in Fig. 1 is of particular interest because it affects the isotopic ratios of the ytterbium isotopes. ^{170}Yb is an s-only isotope that is shielded by stable ^{170}Er from contributions of the r process, and its abundance was measured in pre-solar SiC grains [16]. Focusing on ^{171}Tm, to date only a test measurement was attempted by time of flight at Los Alamos Neutron Science Center (LANSCE), but the neutron scattering background was too large to provide reliable data [17]. In 2003, the MACS at 25 keV was measured via the activation method at Karlsruhe Institute of Technology (FZK) and a value of 350(30) mb was reported [12]. In the latest release of KADONIS (v1) database [18] this result has been extrapolated to $kT = 30$ keV with the energy-dependent cross section from the Hauser-Feshbach model NON-SMOKER [19] to 228(20) mb, which turns into 246(22) mb when it is renormalized by 1.0785, corresponding to the recent increase in the standard ^{197}Au(n, γ) cross section [20]. The comparison of theoretical and recommended values found and literature has revealed a large spread in values.

The present Letter reports hence on the first combined measurement of ^{171}Tm(n, γ) via the time-of-flight method at the CERN n_TOF facility in Switzerland [21] and via activation at the Soreq Nuclear Research Center (SNRC) SARAF-LiLiT facility in Israel [22–24].
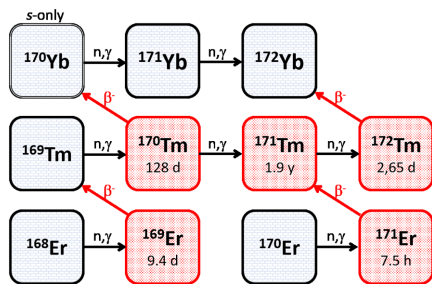

FIG. 1. Scheme of the branching at $A \sim 170$ involving the unstable isotopes ^{169}Er, ^{171}Er, ^{170}Tm, and ^{171}Tm.

The quality of the ^{171}Tm sample has been key to the success of the experiments presented herein. In the context of a larger project involving the production of ^{79}Se, ^{147}Pm, ^{163}Ho, and ^{204}Tl as well, a pellet of 240 mg ^{170}Er$_2$O$_3$ enriched to 98.1% was irradiated for 55 days at the high-flux reactor Institut Laue-Langevin (ILL) in France, where neutron capture on stable ^{170}Er produced sizable quantities of ^{171}Er (7.516 h) that decayed into ^{171}Tm (2.92 y). Following chemical separation and purification at Paul Scherrer Institute (PSI) in Switzerland, the TmO$_2$ composition was 97.91% enriched in ^{171}Tm, with 2.03% of ^{169}Tm and 0.06% of ^{170}Tm. A small fraction of the ^{171}Tm was shipped to the TRIGA research reactor at the Johannes Gutenberg-Universität Mainz in Germany where the thermal and resonance integral capture cross sections were measured for the first time [25]. The remaining Tm$_2$O$_3$ was deposited in circular areas (22 mm in diameter) onto two 5 μm thick Al foils and then placed face-to-face into a 60 mm diameter plastic ring serving as the sample holder [26]. The resulting sample contained, at the beginning of the n_TOF experiment, 3.13(12) mg of ^{171}Tm, a value calculated within 4% by γ-ray spectroscopy from the ^{171}Tm 66.7 keV decay line (the value reported in Ref. [26] has been updated, scaled up by 11%, in light of the new intensity value of the decay line of Ref. [27]).

The time-of-flight experiment was carried out at the CERN n_TOF facility [21]. n_TOF features a pulsed white neutron beam where (n, γ) cross sections are measured as a function of the neutron energy via the time-of-flight technique. The experiment was carried out at the 185 m neutron beam line (EAR-1), where the γ-ray cascades following neutron capture in ^{171}Tm were studied using the total energy technique [28], based on four 620 ml C$_6$D$_6$ detectors [29]. The fraction (N_{SRM}) of the beam intersecting the sample was determined via the saturated resonance method (SRM) [30] for the 4.9 eV resonance of a ^{197}Au sample of the same diameter. The beam-independent (mainly sample activity) and beam-dependent (neutron and photon scattering) background components were assessed by dedicated measurements with Pb, C, and empty samples. The neutron energy distributions from the ^{171}Tm sample and the background measurements are displayed in Fig. 2, with resonances showing up above the background up to 700 eV. It is remarkable that even though n_TOF is one of the facilities with the highest instantaneous neutron beam intensity worldwide, the dominant background in this region is still due to the activity of the sample.

The capture cross section in each energy bin is then determined as

$$\sigma_{n,\gamma}(E_n) = \frac{C_w(E_n) - B_w(E_n)}{n_{at}\varepsilon_{n,\gamma}\Phi_n(E_n)N_{srm}}f_{\text{thr}}^{\text{Au/Tm}}, \tag{1}$$
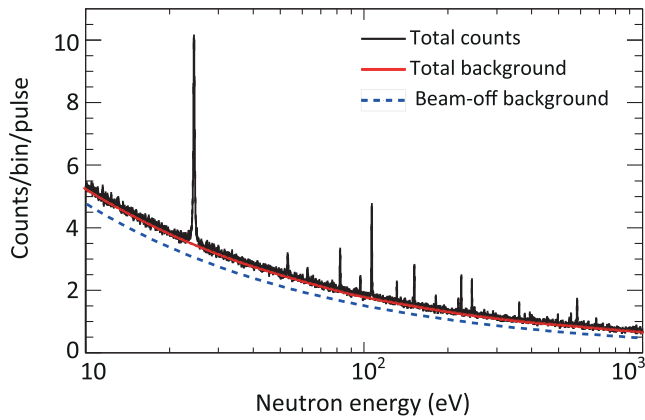
FIG. 2. Distribution of counts as function of the neutron energy during the ^{171}Tm(n, γ) experiment at nTOF. The dominant beam-off background from the activity of the sample does not prevent resolving the individual resonances (see inset).

FIG. 3. Measured (this work) and evaluated (JEFF-3.3, based on TALYS-2015) resonance radiative kernels of ^{171}Tm. The blue dashed-line corresponds to the estimated observation threshold.

where $C_w(E_n)$ and $B_w(E_n)$ are the *weighted* total and background counts per pulse, n_{at} is the areal density of the ^{171}Tm sample, $\phi_n(E_n)$ is the neutron flux expressed as neutrons or pulse [21], $\varepsilon_{n,\gamma}$ is detection efficiency calculated via simulations using the pulse height weighting technique [28], and N_{SRM} has been described above. Last, $f_{thr}^{Au/Tm} = 1.01(1)$ is a correction factor accounting for the effect of the 250 keV detection threshold on the γ-ray cascades from ^{197}Au and ^{171}Tm [15].

The systematic uncertainty of the resulting cross section is 4%, with contributions from the shape (1% below 1 keV) and absolute value (1% from N_{SRM}) of the neutron flux, the detection efficiency (2%), the sample mass (4%), $f_{thr}^{Au/Tm}$ (1%), and last, 2% uncertainty associated with the relative positioning of the ^{171}Tm and ^{197}Au samples in the beam. On the other hand, the statistical uncertainty is quite different from resonance to resonance and dominates over the systematic uncertainty for the majority of the resonances [31].

Each of the 28 observed resonances belonging to ^{171}Tm (the resonances from ^{169}Tm at 4 and ^{171}Yb at 53 eV were neglected) were analyzed and parametrized using the Bayesian R-matrix code SAMMY [32]. The resonance parameters are listed in the Supplemental Material [31].

A careful statistical analysis of these parameters, taking into account the bias related to the weak resonances lost below the observation threshold indicated in Fig. 3, yields the following values for the s-wave level spacing, strength, and average radiative width: $D_0 = 15(4)$ eV, $S_0 = 1.3(4) \times 10^{-4}$, and $\langle \Gamma_\gamma \rangle = 80(9)$ meV. These s-wave values together with an S_1 value of 2×10^{-4} (from systematics) have been plugged into the FITACS code [33] (implemented in SAMMY) to calculate the cross section up to 300 keV, from which a MACS value at 30 keV of 570 (220) mb has been calculated using Eq. (3) in Ref. [2]. The uncertainty of $\sim 38\%$ is dominated by that of the input parameters and can in the future be reduced if more
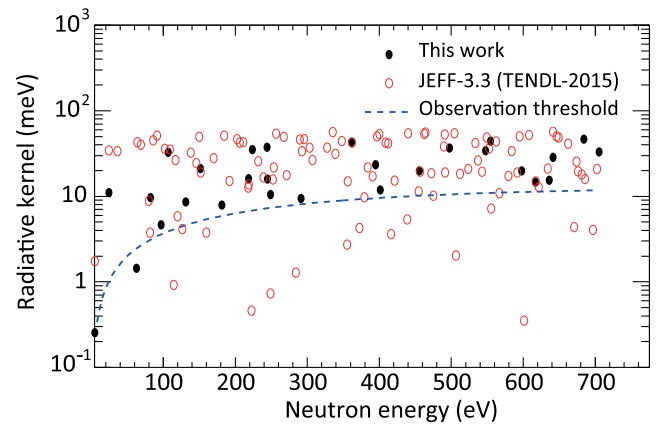
resonances are observed. More information about the n_TOF experiment, the resonance analysis, and the FITACS calculations will be provided in the upcoming detailed paper [34].

Deduced resonance kernels (see Ref. [31]) are compared to values from TALYS-2015 [35] statistical model calculations as given in JEFF-3.3 [36] in Fig. 3. Evidently, the evaluation overestimates their number as well as maximum values, leading to a higher cross section compared to our data (see Fig. 5).

The activation experiments were carried out at the SNRC SARAF using the liquid lithium target (LiLiT) facility [22,23] as a quasi-Maxwellian neutron source. The SARAF accelerator [37,40] features the highest current (2 mA) low energy ($\sim$1.5–4 MeV) proton beam available for neutron production at an energy close to the ^{7}Li$(p, n)^7$Be reaction threshold of 1.88 MeV [24,41]. In order to withstand the high power deposition (3–4 kW), the target is a windowless film (1.5 mm thick) of liquid lithium circulating in a closed loop, serving both for neutron production and as the beam dump.

The ^{171}Tm material from the n_TOF sample was recovered, separated, purified, and deposited on a 0.5 mm thick high purity Al disk (22 mm diameter) and reshipped. The ^{171}Tm sample activity was determined as 24.4(10) GBq [2.13(8) $\times$ 10^{18} ^{171}Tm atoms] at SARAF as done in [26] by the 66.7 keV decay line [27] with a high-purity Ge (HPGe) detector. The sample, encapsulated in an Al holder and positioned at 6.5 mm from the Li surface behind a thin stainless steel wall (see [23] for details), was irradiated in two experiments for which the neutron field was produced by proton beams of 1910 (IR1) and 1946 keV (IR2) with a spread of $\sim$15 keV. A gold monitor foil (22 mm diameter) of 97.2(1) and 107.1(1) mg for IR1 and IR2, respectively, was affixed to the Al sample holder 1 mm upstream of the ^{171}Tm sample. The integrated proton charges of 8.8 and 4.6 mA·h, respectively, were determined by counting
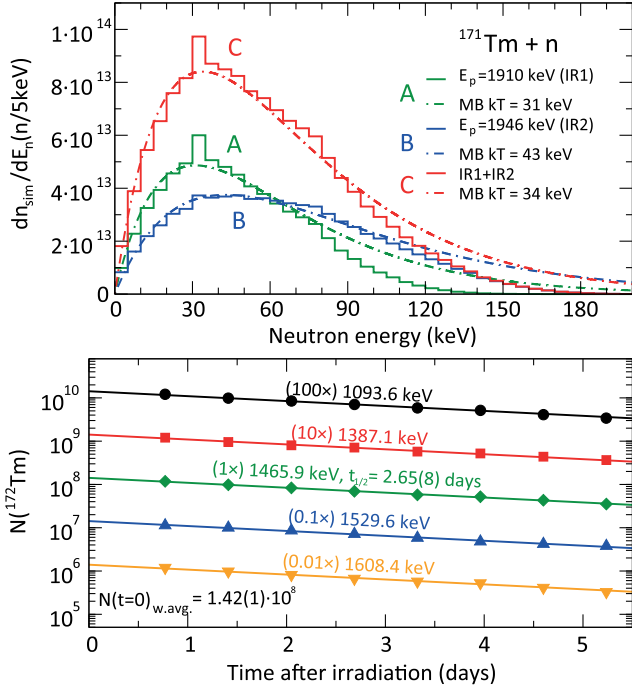
FIG. 4. (top) Simulated neutron spectra impinging on the ^{171}Tm sample (IR1, IR2 and IR1 + IR2) calculated by the SimLiT-GEANT4 simulations fitted by Maxwell-Boltzmann (MB) distributions.; (bottom) Decay curves of five identified lines following the decay of ^{172}Tm after LiLiT activation (IR2). The various decay curves were scaled in order to all fit in one plot. The ^{172}Tm half-life determined by these curves [2.65(8) d] is in perfect agreement with the adopted half-life 2.65(1) d.

neutron-induced fission products in a ^{235}U-loaded detector located at 0°, 70 cm downstream of the sample calibrated at low beam intensity against a Faraday cup. The energy distribution of the neutrons hitting the ^{171}Tm sample was calculated via simulations with the benchmarked SimLiT-GEANT4 code [24,42] for the two cases (Fig. 4, top). The simulated spectra closely resemble a Maxwell-Boltzmann flux distribution (MB) with effective kT values of 31 and 43 keV for the 1910 and 1946 keV proton energies, respectively, slightly underestimating the high energy component, as is common in experiments using the ^{7}Li(p,n) reaction. Also shown in Fig. 4 is the summed spectrum of the two irradiations, strictly representing the energy distribution of all neutrons that activated the sample, fitted with a $kT = 34$ keV MB.

The activities of ^{172}Tm [$t_{1/2} = 2.65(1)$ d] were measured for five days after the irradiation (Fig. 4, bottom). The irradiated ^{171}Tm sample was positioned at 52 mm from a HPGe detector equipped with Pb (6 mm) and Cu (2 mm) absorbers to attenuate the high-intensity low-energy photons dominating the ^{171}Tm activity and the β-induced bremsstrahlung. The efficiency curve was determined within 2% using a multi-gamma (^{85}Sr, ^{137}Cs, ^{88}Y, ^{60}Co) and a ^{152}Eu source in the mentioned geometry and absorber

configuration. The count rates from five transitions following the decay of ^{172}Tm and that of ^{198}Au (412 keV, measured at 5 cm from the same Ge detector), corrected to the end of each irradiation, were used together with the respective efficiency, γ-ray intensity [43,44] and self-shielding (negligible) to extract the number of activated ^{172}Tm (N^{172}) and ^{198}Au (N^{198}) nuclei after irradiation (Fig. 4, bottom). The N^{172} values from the five γ-ray lines agree within 2%, consistent with the 5% relative uncertainty of the transitions. The SimLiT-GEANT4 simulations, calculating also the number of activated ^{198}Au nuclei on a statistically relevant sample [24,45] on the basis of the ENDF/B-VIII ^{197}Au(n,γ) cross sections, agree with the experimentally determined N^{198} nuclei within 1%.

The spectrum-averaged cross section (SACS) of ^{171}Tm for each irradiation was determined using the Au monitor foil as reference through the relation

$$\sigma_{\mathrm{SACS}}(^{171}\mathrm{Tm}) = \sigma_{\mathrm{SACS}}(^{197}\mathrm{Au}) \frac{N^{172}}{N^{198}} \frac{N^{197}}{N^{171}} \frac{f^{\mathrm{Au}}}{f^{\mathrm{Tm}}} f_{\varphi}. \quad (2)$$

In Eq. (2) $N^{171,197}$ are the respective number of ^{171}Tm and ^{197}Au sample nuclei, $f^{\mathrm{Tm,Au}}$, f_{φ} correction factors, respectively, for decay and neutron rate variations during each irradiation and for the different neutron fluence on the ^{171}Tm sample and Au monitor [$f_{\varphi} = 1.02$ (1.05) for IR1 (IR2)]. The SACS of ^{197}Au [$\sigma_{\mathrm{SACS}}(^{197}\mathrm{Au}) = 589(12)$ mb and 510(10) mb for IR1 and IR2, respectively] in Eq. (2) are calculated by the convolution of the JEFF-3.3 ^{197}Au$(n,\gamma)^{198}$Au pointwise cross sections (consistent with [46,47]) with the simulated spectrum for each irradiation. The resulting values of $\sigma_{\mathrm{SACS}}(^{171}\mathrm{Tm})$ are 385(39) and 299 (30) mb for IR1 and IR2, respectively.

The ^{171}Tm(n,γ) SACS values are used to extract the MACS at a thermal energy kT via the equation

$$\sigma_{kT}(^{171}\mathrm{Tm}, kT) = \frac{2}{\sqrt{\pi}} C_{E_n}(kT) \sigma_{\mathrm{SACS}}(^{171}\mathrm{Tm}). \quad (3)$$

In Eq. (3), the factor

$$C_{E_n}(kT) = \frac{\int_0^\infty \sigma_{n,\gamma}(^{171}\mathrm{Tm}, E_n) E_n e^{-E_n/kT} dE_n}{\int_0^\infty E_n e^{-E_n/kT} dE_n}$$
$$\times \frac{\int_0^\infty \frac{dn_{\mathrm{sim}}}{dE_n} dE_n}{\int_0^\infty \sigma_{n,\gamma}(^{171}\mathrm{Tm}, E_n) \frac{dn_{\mathrm{sim}}}{dE_n} dE_n} \quad (4)$$

expresses a correction due to the difference between the thermal energy $kT = 30$ keV and the effective kT value of the experimental spectrum and to the departure of the latter spectrum from a true Maxwellian [$C_{E_n} = 0.93(1)$ and 1.08 (3) for IR1 and IR2, respectively]. The $\sigma_{kT}(^{171}\mathrm{Tm}, 30\,\mathrm{keV})$ values extracted from IR1 and IR2, respectively, 404(41) and 364(38) mb, are consistent with each other, attesting the validity of Eq. (3). We determine our ^{171}Tm MACS

value at 30 keV as 384(40) mb, the average of the two values weighted by the number of neutrons hitting the sample in IR1 and IR2. An equivalent value of 385(40) mb is extracted from the summed neutron spectrum of IR1 and IR2 [Fig. 4 (top)] and the averaged $\sigma_{\mathrm{SACS}}(^{197}\mathrm{Au})$ value for IR1 and IR2 weighted as above. The statistical uncertainty from the γ-ray counting of the samples is negligible (below 1%). The main contributors to the overall systematic uncertainty of 10% were the HPGe detector efficiency (2%), the absolute (8%) and the respective relative $^{172}\mathrm{Tm}$ γ-ray intensity (5%), the $^{171}\mathrm{Tm}$ sample mass (4%), the $^{197}\mathrm{Au}$ reference cross section (1.8%) and the uncertainty estimate (1.5%) of the factors $C_{E_n}(kT)$ assessed by using the two evaluated cross sections available. As a validation of this result, the MACS of stable $^{169}\mathrm{Tm}$ was measured using the same experimental and analysis procedures, resulting in a MACS (30 keV) of 990(60) mb, in agreement within uncertainties with the value of 1065 (65) mb from KADoNiS (v1) [18].

We compare in Fig. 5 the results of these works with theoretical models and experimental results from the literature (see Supplemental Material [31] for the detailed values). The value of 384(40) mb reported herein is 1.6 times larger than that of the KADoNiS (v1) database (renormalized by a factor of 1.0785, see above), which is based on the first and only previous attempt to measure the MACS of $^{171}\mathrm{Tm}$ by activation [12]. The comparison with the value from the differential measurement performed at n_TOF within this work shows that the latter provides a MACS value at 30 keV that, although with limited accuracy and estimated from data only below 700 eV, is in agreement with the activation value within uncertainties. The sizable

cross section overestimation in the evaluations seems to be due to the unrealistically large level density parameter and resonance kernels used in the TALYS-2015 calculations (see Fig. 3), due to the lack of experimental data prior to our measurement. The more recent TALYS-2017 calculation seems to have implemented changes that shift the predictions in the right direction, although this has not been yet adopted in the evaluated nuclear data libraries.

As a first step to evaluate the impact of this new cross section in astrophysics modeling, we have performed stellar model calculations with a 2 solar mass star in its AGB phase with a metallicity of 0.01. These stellar parameters are representative for the production site of presolar SiC grains in the envelopes of C-rich AGB stars.

In Fig. 6 we compare the isotopic ratios of three Yb isotopes as measured in SiC grains from the Murchison meteorite (labeled Mu1, Mur2, and Old Mur; [16]) with four AGB calculations using different $^{171}\mathrm{Tm}$ cross sections: JEFF-3.3 (used as reference), this work, the estimation of Bao *et al.* (commonly used as a reference in nucleosynthesis calculations) and the value proposed in KADoNiS (v1). All models start with a solar-scaled ytterbium composition (see dotted curves marking the solar ratios) and proceed to lower $^{171}\mathrm{Yb}/^{172}\mathrm{Yb}$ and $^{173}\mathrm{Yb}/^{172}\mathrm{Yb}$ ratios, with each dot corresponding to the surface composition following a mixing episode occurring during the AGB phase [the so-called third dredge ups, (TDUs), see, e.g., Ref. [48]]. During TDUs, by-products of nuclear burning occurring in stellar interiors are mixed to the surface, including carbon (produced by the 3α processes) and s-process isotopes. Open dots refer to TDUs after which the C/O ratio is lower than one. These points cannot be directly compared to SiC grains (which form at C-rich
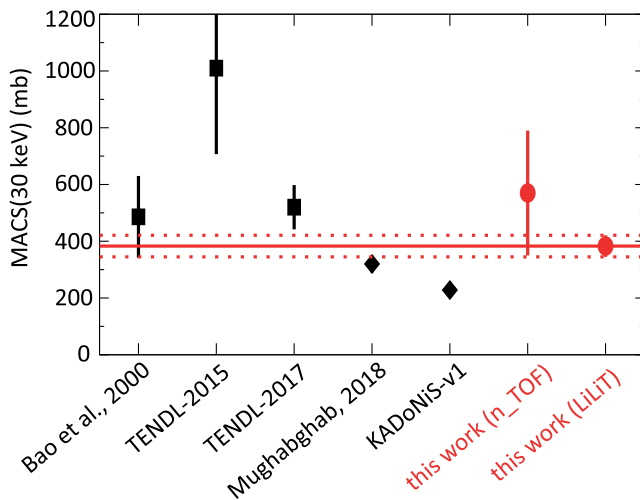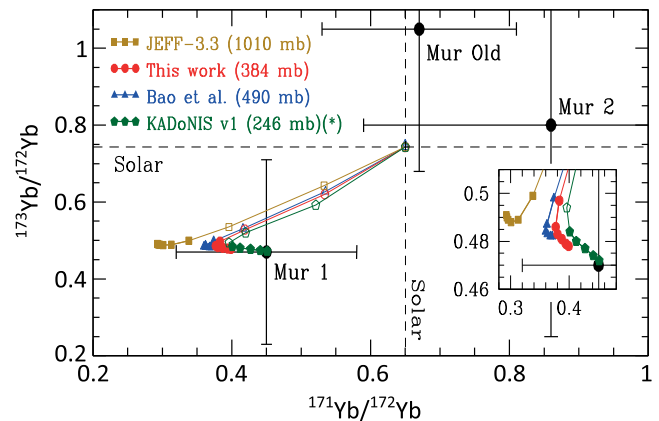

FIG. 5. Comparison of the MACS values at 30 keV from this work (red circles), previous measurements and compilations (black diamond) and theoretical models (black square). The TENDL-2015 value is currently adopted in the JEFF-3.3 evaluation. See Supplemental Material [31] for the detailed values [38,39].

FIG. 6. Isotopic ratios from Yb isotopes observed in a sample of the Murchison meteorite [16] and calculated after each mixing episode, starting form solar, using four different MACS values. (*renormalized by a factor of 1.0785 corresponding to a change in the reference $^{197}\mathrm{Au}$ MACS value).

regimes), but are useful to follow the behavior of the models. Filled dots correspond to TDUs after which SiC grains may form.

During the C-rich phase, the model computed with our new measurement (as well as with the recommended values from Bao *et al.* [38] and KADONIS (v1) [18]) turns to larger ^{171}Yb/^{172}Yb values, with a final value compatible within uncertainties with the Mur1 measurement. On the contrary, the evaluation yields an abundance pattern one sigma away from the Mur1. Note that the ytterbium ratios of the other two grains published by [16] (Mur2 and Mur Old) are consistent to solar ratios. Thus, they have probably been contaminated by solar material and cannot be used as a reference for AGB nucleosynthesis.

The two successful experiments presented herein feature the lowest sample mass, shortest half-life and highest activity samples measured at the CERN *n*_TOF-EAR1 and SARAF-LiLiT facilities to date. Remarkably, although with quite different accuracies, they provide compatible results for the value of interest in astrophysics, the MACS at 30 keV. This bears important implications for future measurements where the compound nucleus $^{A+1}$Z resulting from the (n, γ) reaction is not radioactive, in which case a measurement via the activation technique is not possible. This is the case for some important *s*-process branching points such as ^{85}Kr, ^{147}Nd, ^{151}Sm, ^{153}Gd, ^{185}W, or ^{204}Tl; for these only time-of-flight experiments can provide information about the MACS and, as shown in this work, the experiments are worthwhile even if the energy range that can be studied does not extend up to the tens of keV that are required for astrophysical applications.

*Corresponding author.
cguerrero4@us.es

[1] E. Burbidge, G. Burbidge, W. Fowler, and F. Hoyle, Rev. Mod. Phys. 29, 547 (1957).
[2] F. Käppeler, R. Gallino, S. Bisterzo, and W. Aoki, Rev. Mod. Phys. 83, 157 (2011).
[3] P. Neyskens *et al.*, Nature (London) 517, 174 (2015).
[4] C. Abia, M. Busso, R. Gallino, I. Dominguez, O. Straniero, and J. Isern, Astrophys. J. 559, 1117 (2001).
[5] G. Raskin *et al.*, Astron. Astrophys. 526, A69 (2011).
[6] G. Tagliente *et al.* (*n*_TOF Collaboration), Phys. Rev. C 87, 014622 (2013).
[7] N. Patronis, S. Dababneh, P. A. Assimakopoulos, R. Gallino, M. Heil, F. Käppeler, D. Karamanis, P. E. Koehler, A. Mengoni, and R. Plag, Phys. Rev. C 69, 025803 (2004).
[8] C. Guerrero *et al.*, Phys. Lett. B 797, 134809 (2019).
[9] R. Reifarth, C. Arlandini, M. Heil, F. Kappeler, P. V. Sedyshev, A. Mengoni, M. Herman, T. Rauscher, R. Gallino, and C. Travaglio, Astrophys. J. 582, 1251 (2003).
[10] S. Jaag and F. Käppeler, Phys. Rev. C 51, 3465 (1995).
[11] S. Jaag and F. Käppeler, Astrophys. J. 464, 874 (1996).
[12] R. Reifarth, R. Haight, M. Heil, M. M. Fowler, F. Käppeler, G. G. Miller, R. S. Rundberg, J. L. Ullmann, and J. B. Wilhelmy, Nucl. Phys. A718, 478 (2003).
[13] C. Lederer *et al.* (*n*_TOF Collaboration), Phys. Rev. Lett. 110, 022501 (2013).
[14] M. Weigand *et al.*, Phys. Rev. C 92, 045810 (2015).
[15] U. Abbondanno *et al.* (*n*_TOF Collaboration), Phys. Rev. Lett. 93, 161103 (2004).
[16] Q. Z. Yin, C. T. A. Lee, and U. Ott, Astrophys. J. 647, 676 (2006).
[17] J. L. Ullmann, R. C. Haight, M. M. Fowler, G. G. Miller, R. S. Rundberg, and J. B. Wilhelmy, AIP Conf. Proc. 475, 251 (1999).
[18] Karlsruhe Astrophysical Database of Nucleosynthesis in Stars (v1) https://exp-astro.de/kadonis1.0/.
[19] T. Rauscher and F. K. Thielemann, Atomic Data Nucl. Data Tables 75, 1 (2000).
[20] A. D. Carlson *et al.*, Nucl. Data Sheets 163, 280 (2020).
[21] C. Guerrero *et al.* (*n*_TOF Collaboration), Eur. Phys. J. A 49, 27 (2013).
[22] S. Halfon *et al.*, Rev. Sci. Instrum. 85, 056105 (2014).
[23] M. Paul *et al.*, Eur. Phys. J. A 55, 44 (2019).
[24] M. Tessler *et al.*, Phys. Lett. B 751, 418 (2015).
[25] T. Heftrich *et al.*, Phys. Rev. C 99, 065810 (2019).
[26] S. Heinitz *et al.*, Radiochim. Acta 105, 801 (2017).
[27] I. Kajan, S. Heinitz, R. Dressler, P. Reichel, N. Kivel, and D. Schumann, Phys. Rev. C 98, 055802 (2018).
[28] R. L. Macklin and J. H. Gibbons, Phys. Rev. 159, 1007 (1967).
[29] R. Plag, M. Heil, F. Käppeler, P. Pavlopoulos, R. Reifarth, and K. Wisshak, Nucl. Instrum. Methods Phys. Res., Sect. A 496, 425 (2003).
[30] R. Macklin, J. Halperin, and R. Winters, Nucl. Instrum. Methods Phys. Res., Sect. A 164, 213 (1979).
[31] See Supplemental Material at http://link.aps.org/supplemental/10.1103/PhysRevLett.125.142701 for a detailed list of resonance parameters and their uncertainties.
[32] N. M. Larson, Updated users' guide for SAMMY: Multilevel R-matrix fits to neutron data using Bayes' equations, Report No. ORNL/TM-9179/R8, Oak Ridge National Laboratory, 2008.
[33] F. H. Froehner, Nucl. Sci. Eng. 103, 119 (1989).
[34] J. Lerendegui-Marco *et al.* (to be published).

[35] A. J. Koning, D. Rochman, J. Sublet, N. Dzysiuk, M. Fleming, and S. van der Marck, Nucl. Data Sheets **155**, 1 (2019).

[36] The Joint Evaluated Fission and Fusion File (JEFF) https:// www.oecd-nea.org/dbdata/JEFF33/.

[37] A. Kreisel *et al.*, in *Proceedings of the LINAC2014, Geneva, Switzerland* (CERN, 2014), https://accelconf.web.cern.ch/ linac2014/papers/weiob02.pdf.

[38] Z. Y. Bao, H. Beer, F. Käppeler, F. Voss, K. Wisshak, and T. Rauscher, At. Data Nucl. Data Tables **76**, 70 (2000).

[39] S. F. Mughabghab, *Atlas of Neutron Resonances 6th Edition: Resonance Parameters and Thermal Cross Sections. Z=61–102* (Elsevier 2018), https://www.elsevier .com/books/atlas-of-neutron-resonances/mughabghab/978- 0-444-63780-2.

[40] I. Mardor *et al.*, Eur. Phys. J. A **54**, 91 (2018).

[41] W. Ratynski and F. Käppeler, Phys. Rev. C **37**, 595 (1988).

[42] M. Friedman *et al.*, Nucl. Instrum. Methods Phys. Res., Sect. A **698**, 117 (2013).

[43] B. Singh, Nucl. Data Sheets **75**, 199 (1995).

[44] H. Xiaolong and K. Mengxiao, Nucl. Data Sheets **133**, 221 (2016).

[45] M. Tessler, Ph.D. thesis, Hebrew University of Jerusalem, 2018, http://arad.mscc.huji.ac.il/dissertations/W/JSL/ 9920713243703701.pdf.

[46] C. Lederer *et al.* (n_TOF Collaboration), Phys. Rev. C **83**, 034608 (2011).

[47] C. Massimi *et al.*, Eur. Phys. J. A **50**, 124 (2014).

[48] S. Cristallo, L. Piersanti, O. Straniero, R. Gallino, I. Domínguez, C. Abia, G. Di Rico, M. Quintini, and S. Bisterzo, Astrophys. J. Suppl. Ser. **197**, 17 (2011).